


## Investigation of Pt/Fe-N-C Hybrids Towards ORR in Acidic Environment



To cite this article: Dana Schonvogel *et al* 2022 *ECS Trans.* **109** 401

View the [article online](#) for updates and enhancements.





 The Electrochemical Society  
Advancing solid state & electrochemical science & technology

**242nd ECS Meeting**  
Oct 9 – 13, 2022 • Atlanta, GA, US  
Presenting more than 2,400 technical abstracts in 50 symposia

**ECS Plenary Lecture**  
featuring  
**M. Stanley Whittingham**,  
Binghamton University  
Nobel Laureate –  
2019 Nobel Prize in Chemistry

 **Register now!**



## Investigation of Pt/Fe-N-C Hybrids Towards ORR in Acidic Environment

Dana Schonvogel, Nambi Krishnan Nagappan, Nina Bengen, Julia Müller-Hülstede,  
and Peter Wagner

German Aerospace Center (DLR), Institute of Engineering Thermodynamics,  
Carl-von-Ossietzky-Str. 15, 26129 Oldenburg, Germany

Metal-nitrogen-carbon (M-N-C) compounds such as Fe-N-Cs are currently the most promising platinum group metal free catalysts for oxygen reduction. Regarding the overriding goal of reducing PEM fuel cell production costs by reducing the amount of platinum, the use of Fe-N-Cs as catalytic active support is investigated in this study. Activity and stability of Pt in different contents on a commercial Fe-N-C is compared to Pt on a typical carbon black. Pt nanoparticles are well-distributed on both support classes. However, electrochemical surface and mass activity of Pt is lower on Fe-N-C compared to carbon black. Although Pt does not profit in any catalytic matter from interaction with Fe-N-C, the Pt/Fe-N-C in total has a boosting effect on ORR activity being important for future strategies to lower the Pt content in PEM fuel cells.

### Introduction

Polymer electrolyte membrane fuel cells (PEMFCs) are recognized as one of the renewable energy converters in portable, automobile, and stationary applications. Currently, both low temperature (LT) and high temperature (HT) PEMFCs use platinum group metal (PGM) based catalysts for oxygen reduction reaction (ORR) containing usually Pt nanoparticles on carbon black. To reduce the total cost of PEMFC stack, worldwide researchers have considerable attention to find an inexpensive alternative catalyst. Recently, metal-nitrogen-carbon (M-N-C) compounds such as Fe-N-Cs are the most promising PGM-free catalysts for ORR. However, they suffer from insufficient volumetric activity and electrochemical stability in PEMFCs (1, 2). Xiao et al. have proven an improved electrochemical stability of Pt-Fe-N-C electrocatalysts consisting of atomically dispersed Pt and Fe atoms or Pt-Fe alloy nanoparticles in comparison with Fe-N-C only (3). Mechler et al. have reported that the addition of 1-2 wt.% Pt in hybrid Pt/Fe-N-C catalyst performs well with an increased stability in LT-PEMFCs (4). Liao et al. have recently shown better ORR activity of Pt/Fe-N-C than Pt/C (5).

With the goal of reducing LT- and HT-PEMFC production costs, Pt/Fe-N-C activity and stability with systematically reducing the Pt-content has not been investigated yet. In this study, Pt/Fe-N-C hybrids are synthesized using PMF-011904 from Pajarito Powder (USA) as catalyst support and wet-chemically precipitated Pt nanoparticles with targeted Pt-contents of 40, 5 and 1 wt%. To identify the effect of Fe-N-Cs as support, Pt/C catalysts are synthesized in the same way using Black Pearls® 2000 (C) from Cabot (United States).

First, ICP mass spectrometry is used for Pt quantification along all catalysts, and transmission electron microscopy (TEM) is carried out to investigate morphology and Pt nanoparticle diameter and distribution on the Fe-N-C and C support, respectively. Second, mass activity (MA) of ORR is investigated by rotating disc electrode (RDE) experiments in 0.1 mol L<sup>-1</sup> HClO<sub>4</sub>, and the electrochemical surface area (ECSA) of Pt is calculated by hydrogen underpotential deposition and CO stripping voltammetry. Last, accelerated stress testing (AST) is performed with 5000 triangle potential cycles between 0.6–1.5 V<sub>RHE</sub> to evaluate the catalyst stability.

## Experimental Part

### Catalyst Synthesis

Catalyst supports in this study are Black Pearls<sup>®</sup> 2000 (C) from Cabot (United States) and PMF-011904 from Pajarito Powder (United States). Both supports were used to deposit Pt nanoparticles in targeted contents of 1 wt%, 5 wt% and 40 wt% each. The synthesis of Pt nanoparticles and their deposition were according to literature (6-8). 692 mg of H<sub>2</sub>PtCl<sub>6</sub>·6H<sub>2</sub>O from Alfa Aesar (United States) were put in 88 mL of ethylene glycol from Carl Roth (Germany). 12 mL of a NaOH ethylene glycol mixture in a concentration of 2 mol L<sup>-1</sup> were added to reach an alkaline environment. The mixture was stirred for 4 h at 140 °C to precipitate the nanoparticles. To deposit 40 wt% platinum on the support then, 19.5 mL of nanoparticle suspension were mixed with 40 mL of HCl in a concentration of 1 mol L<sup>-1</sup> and centrifuged for 10 min at 7000 rpm to separate the nanoparticles. Afterwards, particles were washed three times by using fresh HCl solution, and centrifugation was done again. After dispersing the particles in acetone, 60 mg of support was added. To reach the further Pt contents of 1 wt% and 5 wt%, the amount of added support was adapted in appropriate way. The mixture was then sonicated in a sonification bath until complete acetone evaporation. The final catalyst was dried under vacuum overnight, washed with ultrapure water and dried a second time under vacuum overnight.

### Physical Characterization

For TEM the appropriate catalyst powder was dispersed in ethanol, and 5 μL of the dispersion was then dropped onto a copper grid from Plano (Germany) consisting of 200 meshes and being coated with carbon/formvar. Microscopy was then performed using the EM 902A device from Carl Zeiss (Germany) with a tungsten cathode and a CCD camera and an acceleration voltage of 80 kV. The Pt nanoparticle diameter was measured using the ImageJ software and averaged using at least 300 particles.

For inductively coupled plasma mass spectrometry (ICP-MS) 2 mg of catalyst powder was stored overnight in 1.6 mL concentrated HCl from Carl Roth (Germany) and 1.3 mL concentrated HNO<sub>3</sub> from Carl Roth (Germany) to dissolve platinum. Then, the mixture was filtered and diluted using 2 wt% HNO<sub>3</sub> to reach a final volume of 250 mL and the final acidification with nitric acid. Lu ICP standard from Carl Roth (Germany) was added to a final internal standard concentration of 1 mg L<sup>-1</sup>. Pt calibration solutions containing 100, 200, 300, 400, 600 and 800 μg L<sup>-1</sup> were prepared using a Pt ICP standard from Carl Roth (Germany). The measurement was performed using the XSeries2 device from Thermo Fisher Scientific (Germany). During calibration a correlation factor of at least 0.999 was

ensured, and signal intensities of the  $^{194}\text{Pt}$ ,  $^{195}\text{Pt}$  and  $^{196}\text{Pt}$  isotopes were used to calculate the Pt concentrations.

### Electrochemical Characterization

To electrochemically characterize and compare the catalysts of this study RDEs with a glassy carbon disc consisting of an area of  $0.2475\text{ cm}^2$  from Pine were used in a three-electrode setup. While the reference electrode was the reversible hydrogen electrode (RHE) of the type HydroFlex from Gaskatel (Germany), a platinum wire was used as counter electrode. This three-electrode setup was connected to the Autolab PGSTAT128N potentiostat from Metrohm (Germany) equipped with the Nova 2.1 software to perform electrochemical measurements of three identically prepared RDEs for each catalyst.

Therefore, these electrodes were polished through aluminum oxide particle suspensions of the type MicroPolish 40-10081 from Bühler (Switzerland) with particle diameters of  $1.00\text{ }\mu\text{m}$  first and  $0.05\text{ }\mu\text{m}$  second and then coated with appropriate catalyst inks. These inks consist of 6 mg of catalyst powder, 1.99 mL  $\text{H}_2\text{O}$ , 0.5 mL 2-propanol and 20  $\mu\text{L}$  of 5 wt% Nafion<sup>®</sup> in aliphatic alcohol and water dispersion from Sigma Aldrich (Germany). To achieve a homogenous suspension inks were sonicated for 15 min in a sonication bath and by horn-sonication for 4 min (intervals of 30 s switched on and 30 s switched off). A volume of 10.3  $\mu\text{L}$  of ink was dropped on the RDE which was then rotated using 700 rpm for drying and final coating with  $100\text{ }\mu\text{g cm}^{-2}$  of total catalyst amount to keep the coating amount constant independent of the Pt content in the different catalysts. Perchloric acid from Sigma Aldrich (Germany) in a concentration of  $0.1\text{ mol L}^{-1}$  presented the electrolyte during these measurements. Measurements were then carried out using the same following procedure.

First, the electrolyte was rinsed with  $\text{N}_2$  for 15 min for saturation. Second, cyclic voltammetry (CV) at  $0.05\text{-}1.20\text{ V}_{\text{RHE}}$  with a scan rate of  $0.5\text{ V s}^{-1}$  was performed until a steady-state was achieved. Third, the initial characterization was done. This included three CV curves at  $0.05\text{-}1.05\text{ V}_{\text{RHE}}$  with a scan rate of  $0.05\text{ V s}^{-1}$  to determine the ECSA later and further three CV curves at  $0.05\text{-}1.15\text{ V}_{\text{RHE}}$  with a scan rate of  $0.005\text{ V s}^{-1}$  to carry out capacitive background corrections later. After CV, CO stripping voltammetry was carried out. Therefore, the electrolyte was purged with CO for 1 min and with  $\text{N}_2$  for 20 min during applying a constant potential of  $0.15\text{ V}_{\text{RHE}}$  to record afterwards a CV curve at  $0.05\text{-}0.3\text{ V}_{\text{RHE}}$  with a scan rate of  $0.05\text{ V s}^{-1}$ . This verified complete Pt surface poisoning. Then, the actual CO stripping took place by CV at  $0.15\text{-}1.05\text{ V}_{\text{RHE}}$  with a scan rate of  $0.05\text{ V s}^{-1}$ . After CO stripping, electrochemical impedance spectroscopy recorded at  $0.5\text{ V}_{\text{RHE}}$  in range of  $100\text{ kHz}\text{-}0.1\text{ Hz}$  was applied to measure the electrolyte resistance. For following ORR, the electrolyte was rinsed with  $\text{O}_2$  for 20 min followed by recording three CV curves during rotation using 1600 rpm. CV was performed at  $0.05\text{-}1.15\text{ V}_{\text{RHE}}$  with a scan rate of  $0.005\text{ V s}^{-1}$ .

After this initial characterization, the electrolyte was rinsed again using  $\text{N}_2$  for 20 min to apply an accelerated stress test (AST). This included 5000 cycles between  $0.6\text{-}1.5\text{ V}_{\text{RHE}}$  with a scan rate of  $0.5\text{ V s}^{-1}$ . Last, the characterization above was repeated at the end of the procedure to assess catalyst degradation or stability. ECSAs and mass activities were calculated by considering the three identically measured electrodes in each case according to our previous studies (9, 10).

## Results and Discussion

### Physical Characterization

Figure 1 depicts TEM images of the six catalysts with different Pt contents in comparison. Due to low Pt contents the 1 wt% and 5 wt% Pt catalysts mainly show the carbon supports under the microscope, whereas the 40 wt% Pt catalysts show well-distributed Pt nanoparticles on the supports. This verifies sufficient interaction of the Pt nanoparticles with the support in both cases. Next to distributed Pt nanoparticles differences in carbon support morphologies become visible. While Black Pearls (C) consist of the typical carbon particles with diameters of 10-40 nm resulting in larger aggregates, PMF (Fe-N-C) has a more visible inner-porous structure.

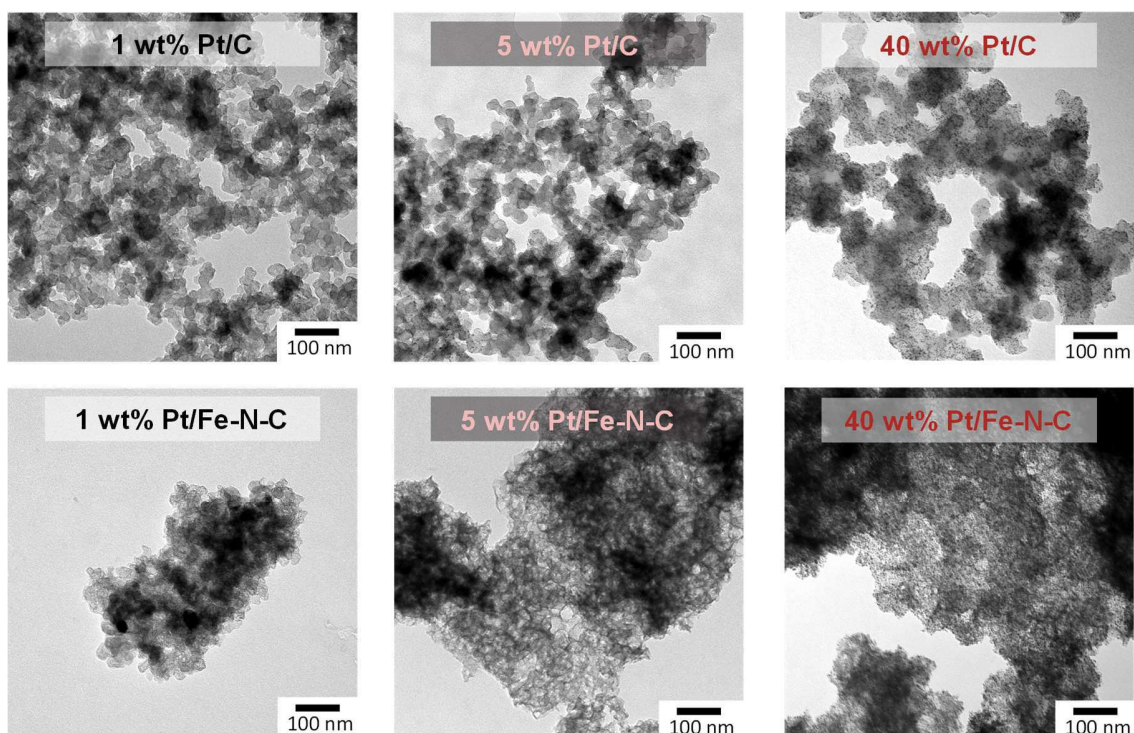


Figure 1. TEM images of catalysts with different Pt contents.

Table I shows the Pt content of all catalysts analyzed by ICP-MS and the averaged diameters of Pt nanoparticles analyzed by TEM. ICP-MS reveals values slightly lower than the targeted content in most cases and a larger value than the targeted content in case of 1 wt% Pt/Fe-N-C. The trend of increasing Pt contents from 1 wt% to 5 wt% and 40 wt% is clearly visible for both supports C and Fe-N-C so that the impact of support and of increasing Pt contents on the ECSA and the ORR can be investigated via electrochemical characterization below. There, the real Pt amounts from this Table I are considered during determination of ECSAs and mass activities for ORR below and ensure high comparability of these electrochemical results. Averaged diameters of Pt nanoparticles are analyzed by TEM for 5 wt% and 40 wt% catalysts and are compared in Table I. The 1 wt% catalysts

contain very little platinum verified by ICP-MS. The very few Pt nanoparticles being visible under microscope make averaging of 300 nanoparticle diameters not feasible. The 5 wt% Pt catalysts show diameters of about 1.20 nm and 1.02 nm, and the 40 wt% Pt catalysts show diameters of about 1.22 nm and 2.02 nm which is the typical range expected from the polyol synthesis in previous studies (9, 11).

**TABLE I.** Pt content (measured through ICP-MS) and averaged Pt diameter (measured through TEM).

Catalyst	Pt content / wt. %	Pt diameter / nm
1 wt% Pt/C	0.4	-
5 wt% Pt/C	3.8	1.20 ± 0.42
40 wt% Pt/C	38.6	1.22 ± 0.48
1 wt% Pt/Fe-N-C	1.4	-
5 wt% Pt/Fe-N-C	4.0	1.02 ± 0.34
40 wt% Pt/Fe-N-C	38.1	2.02 ± 0.54

### Electrochemical Characterization

After physical characterization, the catalysts are electrochemically investigated towards their ECSA and activity for the ORR. These parameters are determined before and after accelerated stress testing to evaluate stabilities. Figure 2 compares CV curves and CO stripping voltammetry curves and the corresponding ECSAs along all catalysts. Figure 2a) and b) reveal that faradaic and capacitive current densities recorded during cyclic voltammetry are lower for Pt/Fe-N-Cs than for Pt/Cs along all Pt content cases. Because total catalyst amounts on the electrodes are kept the same, this indicates lower electrode capacity of Pt/Fe-N-Cs on the one hand and lower electrochemical Pt nanoparticle availability on Fe-N-Cs based on PMF from Pajarito Powder than on Black Pearls® 2000 on the other hand. In case of both 1 wt% Pt catalysts the characteristic Pt peaks with hydrogen underpotential deposition (HUPD) are not detectable which was expected due to very low Pt content. Therefore, ECSA calculation in Figure 2e) is not possible later. Here, CO stripping is more sensitive due to stronger adsorption on Pt surface so that in Figure 2f) ECSA determination is carried out for all catalysts. The CV curves in Figure 2a) and b) after AST show HUPD peak decreases and hydroquinone/quinone peaks increases which is well-known for Pt catalyst degradation as well as carbon support degradation (11-14).

Figure 2c) and d) depict the CO stripping curves and also show lower current densities for Pt/Fe-N-Cs than for Pt/Cs along all Pt content cases in terms of CO oxidation. Another interesting trend in dependence on the Pt content gets obvious here for both supports likewise. Whereas the 1 wt% Pt catalysts show negligible peaks of CO oxidation, the 5 wt% and 40 wt% Pt catalysts show same trends in changing of peak shapes before and after AST. This seems independent of the C or Fe-N-C support. For 40 wt% Pt/C and Pt/Fe-N-C the peak shape changes from one symmetric signal before AST to three strongly overlapped main signals with much lower intensity than the initial signal.

Peak maximums before AST are centered at 0.849  $V_{RHE}$  for Pt/C and at 0.824  $V_{RHE}$  for Pt/Fe-N-C. Peak maximums of the three signals after AST are at 0.751  $V_{RHE}$ , 0.828  $V_{RHE}$  and 0.890  $V_{RHE}$  for Pt/C and at 0.729  $V_{RHE}$ , 0.831  $V_{RHE}$  and 0.926  $V_{RHE}$  for Pt/Fe-N-C. These signals indicate typical Pt particle degradation in terms of agglomeration after AST (15) and show that the electrochemically provoked change of size, shape and surface of Pt particles here is not influenced by the supports to a larger extent. This shows a minor effect

of carbon structure with incorporated Fe-N and N sites here. For 5 wt% Pt/C and Pt/Fe-N-C the peak shape changes from one signal to a very broad low intensity signal which might be the overlap of several peaks again. Peak maximums of 5 wt% Pt catalysts before AST are at  $0.818 V_{\text{RHE}}$  for Pt/C and at  $0.814 V_{\text{RHE}}$  for Pt/Fe-N-C. These very similar CO oxidation behavior with similar peak centers show again comparable size, shape and surface of Pt nanoparticles on both supports in comparison. This is expected due to the same catalyst preparation in this study which includes a separate Pt nanoparticle synthesis first and the deposition on the support second.

ECSAs in Figure 2e) and f) are calculated based on HUPD and CO stripping. In general, higher standard deviations for 5 wt% and 40 wt% Pt/Fe-N-Cs are observed compared to Pt/C which might be due to more inhomogeneous Pt nanoparticle distribution on the bulk support. Next to higher standard deviations, the  $\text{ECSA}_{\text{HUPD}}$  and  $\text{ECSA}_{\text{CO}}$  values are lower for Pt/Fe-N-Cs than for Pt/C along all Pt content cases. This proves the assumption of lower electrochemical Pt nanoparticle availability on Fe-N-Cs above and combines this assumption with a more inhomogeneous Pt availability on Fe-N-Cs. The 40 wt% Pt/C in this study has an  $\text{ECSA}_{\text{HUPD}}$  value of  $94 \pm 5 \text{ m}^2 \text{ g}_{\text{Pt}}^{-1}$  and an  $\text{ECSA}_{\text{CO}}$  value of  $76 \pm 8 \text{ m}^2 \text{ g}_{\text{Pt}}^{-1}$ . This is in range of literature values ranging between 59-125  $\text{m}^2 \text{ g}_{\text{Pt}}^{-1}$  (16). The 40 wt% Pt/Fe-N-C in comparison has an  $\text{ECSA}_{\text{HUPD}}$  value of  $47 \pm 14 \text{ m}^2 \text{ g}_{\text{Pt}}^{-1}$  and an  $\text{ECSA}_{\text{CO}}$  value of  $38 \pm 8 \text{ m}^2 \text{ g}_{\text{Pt}}^{-1}$ .

Although ECSAs of Fe-N-C-based catalysts are lower here compared to C-based catalysts, the Pt/Fe-N-Cs show much lower loss of ECSA after AST and in consequence a better stability than Pt/Cs for 5 wt% and 40 wt% catalysts in CO stripping and for 40 wt% catalysts in HUPD. The determination of ECSAs in case of the low 1 wt% content catalysts is difficult and has low significance due to low signal intensities during CV.

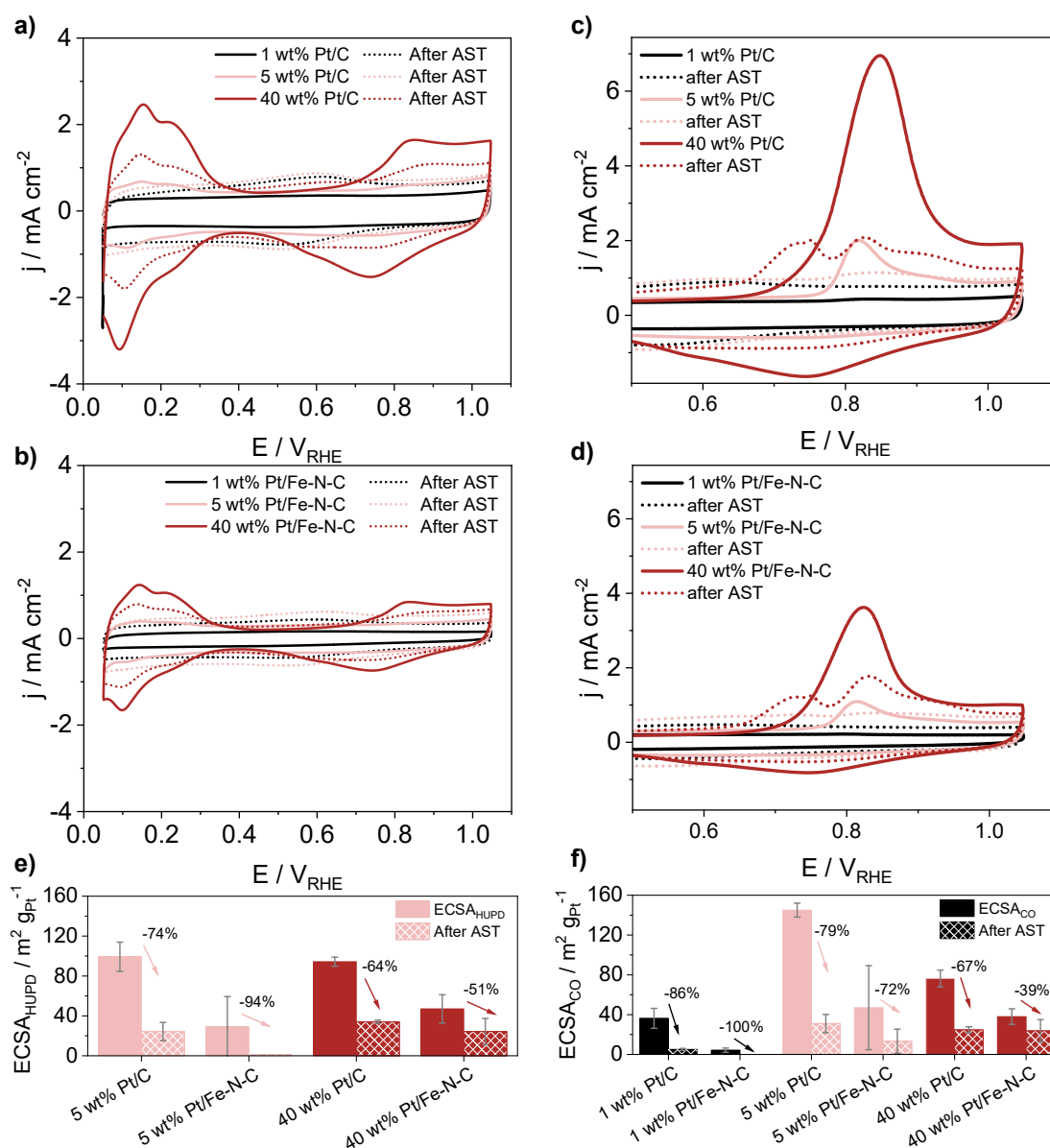


Figure 2. a,b) CVs for determination of ECSA<sub>HUPD</sub> with e) corresponding ECSA values, and c,d) CO stripping voltammetry for determination of ECSA<sub>CO</sub> with f) corresponding ECSA values.

Figure 3 compares the ORR curves as well as the mass and specific activities before and after AST. These curves and activities are shown for the three Pt/C catalysts and the three Pt/Fe-N-C catalysts with 1 wt%, 5 wt% and 40 wt% Pt contents. In addition, the platinum-free Fe-N-C catalyst only is shown to assess the ORR without the presence of platinum. While 40 wt% Pt/C and 40 wt% Pt/Fe-N-C show the expected diffusion limited current density of around  $-6 \text{ mA cm}^{-2}$  typical for Pt catalysts, the others show a successive reducing trend of diffusion limited current densities dependent on the Pt content but independent of the support. Impact factors for this diffusion limited potential region below  $0.6 V_{RHE}$  are uniformity of coverage of the electrode with catalyst material depending on different support morphologies and Pt loading, electrical conductivities and ORR



mechanism (17, 18). Next to the typical Pt loading of 40 wt% very low contents are investigated in this study, whereas the total amount of Pt/support instead of Pt only is kept constant to avoid very thick films on the electrodes. This might result in more distinct impacts of support material by decreasing the Pt content.

Next to this region, the range at higher potentials above around 0.6  $V_{\text{RHE}}$  shows much lower current densities and is rather dominated by catalytic activity than diffusion. To better compare, mass activities are calculated at 0.9  $V_{\text{RHE}}$  for all catalysts and at 0.7  $V_{\text{RHE}}$  for 1 wt% Pt/C, 1 wt% Pt/Fe-N-C and Fe-N-C only due to the relatively low activity. Values at 0.9  $V_{\text{RHE}}$  are shown in Figure 3c) and reveal same trends observed for ECSAs. This means that mass activities of Pt/Cs are higher than activities of Pt/Fe-N-Cs in all cases. 40 wt% Pt/C has a mass activity of 352  $\text{A g}_{\text{Pt}}^{-1}$  which is comparable with literature values of commercial Pt/Cs ranging between 200-650  $\text{A g}_{\text{Pt}}^{-1}$  (16). Although Pt nanoparticle interaction with heteroatom-containing sites like nitrogen was shown in other studies to enhance the ORR activity because of greater electron density (19, 20), this positive effect is not visible for Pt/Fe-N-Cs here.

Looking on the loss of activity, MA losses are higher in case of Pt/Cs than in case of Pt/Fe-N-Cs so that Pt on Fe-N-Cs seems more stable. This can be caused by stabilizing effects of nitrogen doping and Fe-N incorporation into the carbon support which can have a different electronic interaction with the deposited Pt nanoparticles than carbon only (21).

Figure 3d) shows mass activities at 0.7  $V_{\text{RHE}}$  for the low content Pt catalysts compared to Fe-N-C based on the mass of total catalyst. Oxygen reduction starts at lower potentials for these catalysts than for the others because of larger overpotentials so that a potential of 0.7  $V_{\text{RHE}}$  is chosen for calculation here. It is illustrated that the use of Fe-N-C support for low Pt content catalysts instead of C only has a boosting effect on ORR activity by factor of two.

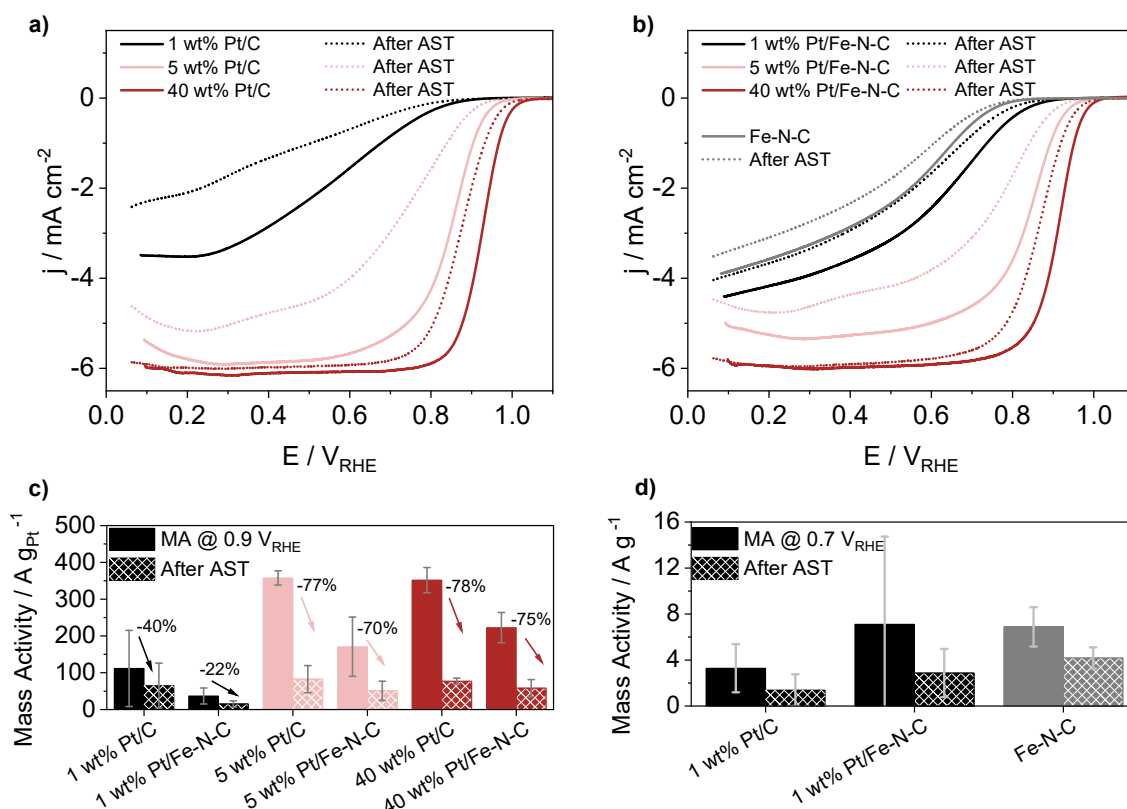


Figure 3. ORR polarization curves of a) Pt/C and b) Pt/Fe-N-C catalysts at 1600 rpm with a scan rate of  $5 \text{ mV s}^{-1}$ , c) mass activities determined at  $0.9 V_{\text{RHE}}$  based on mass of platinum and d) at  $0.7 V_{\text{RHE}}$  based on mass of total Pt/support catalyst.

## Conclusion

In this study, the successful deposition of fabricated Pt nanoparticles on a carbon black and on Fe-N-C in different amounts is shown. The catalysts are analyzed by TEM and ICP-MS and furthermore electrochemically analyzed to compare ECSAs and catalytic activities. Although Pt nanoparticles are well-distributed on both support classes, electrochemical results reveal differences in Pt behavior on the supports. ECSAs and MAs of platinum are lower on Fe-N-Cs than on carbon only. In conclusion, the electronic structure of Pt does not profit in any catalytic matter from interaction with Fe-N and N sites. However, considering not only the mass of platinum but also the total mass of Pt and support, the use of Fe-N-C instead of C has a boosting effect on ORR activity. In case of the low Pt content catalysts activity increase by factor of two is shown, which can get important for future strategies to decrease the Pt content by maintaining the catalytic activity and PEM fuel cell performance. To conclude, the combination of catalytic active Pt with catalytic active Fe-N sites has a synergetic effect on the overall ORR activity. Furthermore, the stability of Pt on Fe-N-C is higher compared to Pt/C, so that Fe-N-Cs can help to increase the overall PEMFC catalyst stability. In further approaches, these catalysts will be tested in HT-PEMFC single cells with the aim to reduce the Pt amounts in gas diffusion electrodes.

### Acknowledgments

This study is in frame of the project HT-PEM 2.0 with the grant number 03ETB016A funded by the Federal Ministry for Economic Affairs and Climate Action on the basis of a decision by the German Bundestag. The authors thank the Electron and Light Microscopy Service Unit of the School of Mathematics and Science of the Carl von Ossietzky University for the use of the imaging facilities and, moreover, Levi Laurenz Schlüschen (DLR) for support in synthesizing Pt nanoparticles.

### References

1. T. Reshetenko, A. Serov, M. Odgaard, G. Randolph, L. Osmieri, and A. Kulikovskiy, *Electrochem. Commun.*, **118**, 106795 (2020).
2. Y. He, S. Liu, C. Priest, Q. Shi, and G. Wu, *Chem. Soc. Rev.*, **49**, 3484 (2020).
3. F. Xiao, G.-L. Xu, C.-J. Sun, I. Hwang, M. Xu, H.-w. Wu, Z. Wei, X. Pan, K. Amine, and M. Shao, *Nano Energy*, **77**, 105192 (2020).
4. A. K. Mechler, N. R. Sahraie, V. Armel, A. Zitolo, M. T. Sougrati, J. N. Schwämmlein, D. J. Jones, and F. Jaouen, *J. Electrochem. Soc.*, **165**, F1084 (2018).
5. W. Liao, S. Zhou, Z. Wang, F. Liu, H. Pan, T. Xie, and Q. Wang, *ChemCatChem*, **13**, 4925 (2021).
6. Y. Wang, J. W. Ren, K. Deng, L. L. Gui, and Y. Q. Tang, *Chem Mater*, **12**, 1622 (2000).
7. R. Kou, Y. Y. Shao, D. H. Mei, Z. M. Nie, D. H. Wang, C. M. Wang, V. V. Viswanathan, S. Park, I. A. Aksay, Y. H. Lin, Y. Wang, and J. Liu, *J Am Chem Soc*, **133**, 2541 (2011).
8. M. Inaba, J. Quinson, J. R. Bucher, and M. Arenz, *Jove-J Vis Exp* (2018).
9. D. Schonvogel, J. Hülstede, P. Wagner, I. Kruusenberg, K. Tammeveski, A. Dyck, C. Agert, and M. Wark, *J Electrochem Soc*, **164**, F995 (2017).
10. A. Dushina, H. Schmies, D. Schonvogel, A. Dyck, and P. Wagner, *Int J Hydrogen Energ*, **45**, 35073 (2020).
11. D. Schonvogel, J. Hülstede, P. Wagner, A. Dyck, C. Agert, and M. Wark, *Journal of The Electrochemical Society*, **165**, F3373 (2018).
12. D. Schonvogel, J. Hülstede, P. Wagner, I. Kruusenberg, K. Tammeveski, A. Dyck, C. Agert, and M. Wark, *J. Electrochem. Soc.*, **164**, F995 (2017).
13. K. Kinoshita and J. Bett, *Carbon*, **11**, 237 (1973).
14. J. Speder, A. Zana, I. Spanos, J. J. K. Kirkensgaard, K. Mortensen, and M. Arenz, *Electrochem. Commun.*, **34**, 153 (2013).
15. S. Taylor, E. Fabbri, P. Levecque, T. J. Schmidt, and O. Conrad, *Electrocatalysis*, **7**, 287 (2016).
16. S. S. Kocha, K. Shinozaki, J. W. Zack, D. J. Myers, N. N. Kariuki, T. Nowicki, V. Stamenkovic, Y. J. Kang, D. G. Li, and D. Papageorgopoulos, *Electrocatalysis*, **8**, 366 (2017).
17. K. J. J. Mayrhofer, D. Strmcnik, B. B. Blizanac, V. Stamenkovic, M. Arenz, and N. M. Markovic, *Electrochim. Acta*, **53**, 3181 (2008).
18. G. Cognard, G. Ozouf, C. Beauger, I. Jiménez-Morales, S. Cavaliere, D. Jones, J. Rozière, M. Chatenet, and F. Maillard, *Electrocatalysis*, **8**, 51 (2017).
19. D. R. Kauffman and A. Star, *Analyst*, **135**, 2790 (2010).

20. M. N. Groves, A. S. W. Chan, C. Malardier-Jugroot, and M. Jugroot, *Chem. Phys. Lett.*, **481**, 214 (2009).
21. P. Stonehart, *Carbon*, **22**, 423 (1984).